JOURNAL OF GEOPHYSICAL RESEARCH, VOL. 115, A06210, doi:10.1029/2009JA015028, 2010

Evolution of plasma sheet particle content under different interplanetary magnetic field conditions

Chih-Ping Wang,[1] Larry R. Lyons,[1] Tsugunobu Nagai,[2] James M. Weygand,[3] and A. T. Y. Lui[4]

Received 27 October 2009; revised 11 January 2010; accepted 29 January 2010; published 19 June 2010.

[1] We have statistically analyzed Geotail data to investigate the processes that result in a plasma sheet that is denser under a prolonged northward than southward interplanetary magnetic field (IMF) period. The observations show that the change of number density with the IMF conditions is mainly due to the changes of particle number per unit magnetic flux (particle content N), with N increasing (decreasing) as the period of northward (southward) IMF extends. The changes are quicker in the first ~2 to 4 h then substantially slow down. The Y profiles show that N is always lowest around midnight and becomes higher toward the flanks. The observed plasma velocities suggest that plasma sheet particles undergo earthward and flankward drift transport, as well as diffusive transport resulting from drift fluctuations. The diffusion coefficients associated with fluctuating drift are estimated to be ~10^5 to 10^6 km^2/s. We have simulated evolution of N resulting from drift and diffusive transport with particle sources along the flanks. The simulation results show that the observed temporal and Y variations of N under different IMF conditions can be accounted for by the competition between the particle increase owing to particles diffusing toward midnight from the flank sources and the particle decrease owing to particles drifting away from midnight. As the IMF turns northward (southward), it is mainly the strengthening (weakening) of diffusive transport owing to the increase (decrease) of the flank source that results in the increase (decrease) of N.

Citation: Wang, C.-P., L. R. Lyons, T. Nagai, J. M. Weygand, and A. T. Y. Lui (2010), Evolution of plasma sheet particle content under different interplanetary magnetic field conditions, *J. Geophys. Res.*, *115*, A06210, doi:10.1029/2009JA015028.

1. Introduction

[2] One of the most significant differences seen in the plasma sheet between northward IMF (N IMF) and southward IMF (S IMF) periods is that the plasma sheet is colder and denser during N IMF [e.g., *Terasawa et al.*, 1997]. These changes in the plasma sheet state have fundamental effects on magnetospheric dynamics and magnetosphere-ionosphere coupling. For example, the colder and denser plasma sheet built up during a N IMF prestorm period can provide more source particles for the ring current, thus likely leading to a stronger ring current, than does a less dense prestorm S IMF plasma sheet [*Lavraud et al.*, 2006; *Lavraud and Jordanova*, 2007; *Chen et al.*, 2007]. Also, modeling of magnetosphere-ionosphere electric coupling has indicated that shielding of the penetration electric field during a convection enhancement is stronger if the proceeding plasmas sheet is colder and denser [e.g., *Gkioulidou et al.*, 2009]. However, the underlying processes responsible for the changes in the plasma sheet with different IMF conditions have not been fully determined.

[3] The transition between a denser plasma sheet under N IMF and a tenuous one under S IMF does not occur immediately as the IMF B_z switches direction [*Terasawa et al.*, 1997; *Øieroset et al.*, 2003]. Low-altitude observations showed that plasma sheet densities increase rather gradually following the IMF becoming northward [*Wing et al.*, 2005], and the density change is mostly associated with a < ~1 keV cold population, which is most often seen well separated from the nominal thermal plasma sheet population (~a few to 10 keV) near the flanks. There is also a large variation in density across the tail with higher densities near the flanks than midnight [e.g., *Wing and Newell*, 2002; *Wang et al.*, 2006]. The above observed temporal and spatial density variations can result from either changes of particle number per unit magnetic flux (particle content), change of flux tube volume per unit magnetic flux, or both. *Wang et al.* [2009]

[1]Department of Atmospheric and Oceanic Sciences, University of California, Los Angeles, California, USA.
[2]Department of Earth and Planetary Sciences, Tokyo Institute of Technology, Tokyo, Japan.
[3]Institute of Geophysics and Planetary Physics, University of California, Los Angeles, California, USA.
[4]Applied Physics Laboratory, Johns Hopkins University, Laurel, Maryland, USA.

0148-0227/10/2009JA015028

showed that there are significant differences in particle content between periods of low and high convection strengths, while the differences in flux tube volumes are not as significant. The goal of this paper is to determine quantitatively the evolution of the cross-tail profiles of plasma sheet particle content after the IMF B_z switches direction, and what are the underlying processes responsible for the variations.

[4] The flanks are believed to be the major source locations for cold plasma sheet particles. This flank source is likely created by magnetosheath particles that enter the magnetosphere by either directly crossing the magnetopause through processes such as Kelvin-Helmholtz vortices [e.g., *Fujimoto and Terasawa*, 1994; *Otto and Nykyri*, 2003] and diffusion [*Johnson and Cheng*, 1997], or through high-latitude reconnection [e.g., *Song and Russell*, 1992; *Li et al.*, 2008]. All the above mechanisms predict the flank sources to be stronger for N than S IMF, suggesting that change of the flank source strength with IMF direction likely plays an important role in the changes of plasma sheet particle content.

[5] That the cold population can be seen extending from the flanks to midnight indicates that there are transport processes allowing the cold particles to have access from the flanks to midnight. Analysis of transport paths shows that electric drift delivers particles toward the earth and the flanks, and thus cannot bring the flank source particles across the tail to midnight [*Wang et al.*, 2007, 2009]. There are some particles from the dawn flank that can move into the midnight plasma sheet owing to magnetic drift [*Spence and Kivelson*, 1993; *Wang et al.*, 2004], however, magnetic drift is too small to move cold particles into the plasma sheet from the dawn flank. In addition, magnetic drift, being directed duskward, cannot transport cold ions from the dusk flank toward midnight. It has been proposed [e.g., *Terasawa et al.*, 1997; *Antonova*, 2006] that diffusion may transport cold particles from the flanks deep into the plasma sheet. In MHD simulations, cold and dense plasma sheet can form under N IMF owing to numerical diffusion [e.g., *Li et al.*, 2008]. Despite diffusion not being physically simulated in the MHD, it nevertheless suggests the likely role of diffusive transport in forming the cold plasma sheet. The plasma sheet flow is constantly fluctuating even during quiet times [e.g., *Angelopoulos et al.*, 1993], and the fluctuation can result in diffusive particle transport if particle number has a spatial gradient. The diffusion coefficient associated with flow fluctuations in the plasma sheet has been estimated [*Borovsky et al.*, 1997, 1998; *Ovchinnikov et al.*, 2000; *Nagata et al.*, 2008]. However, the efficiency of diffusive transport of particles from the flanks, which depends on both the distributions of the diffusion coefficients and particle spatial gradients, has not been quantitatively evaluated to determine if it is capable of bringing enough particles to form the observed dense plasma sheet during N IMF.

[6] In this study, we statistically analyze 11 years of Geotail data to determine the temporal and Y profiles of particle content, perpendicular drift velocities, and the diffusion coefficients for different IMF B_z conditions. We then use the observed drift velocities and diffusion coefficients, as well as flank particle sources established from the observations, to simulate the evolution and spatial distributions of particle content owing to drift and diffusive transport for N and S IMF conditions. We compare the simulation results with the observations to determine if these processes can quantitatively account for the observed evolution and Y profiles of the plasma sheet under different IMF conditions.

2. Plasma Sheet and Solar Wind Data

[7] We use Geotail data in aberrated GSM coordinates (with the aberration angle determined by one hour averaged solar wind velocity) from 1 January 1995 to 31 December 2005 and in the area $|Y| \leq 20\ R_E$ and $-20 \geq X \geq -30\ R_E$. Plasma data from two instruments onboard Geotail are used: the ion and electron data from the Low-Energy Particle (LEP) instrument [*Mukai et al.*, 1994] that covers the ion energy range from 21 eV/q to 44 keV/q and the electron energy range from 43 eV to 41 keV, and the proton data from the Energetic Particles and Ion Composition (EPIC) instrument [*Williams et al.*, 1994] that covers the energy range from 46 keV to 3005 keV. The ion moments are from a summation of the LEP and EPIC data. Magnetic field data is from the magnetic field (MGF) experiment [*Kokubun et al.*, 1994]. The plasma sheet is centered at the equatorial plane. Central plasma sheet crossings in this study are defined by plasma pressure ($P_{ion} + P_{electron}$) being larger than magnetic pressure ($P_{mag} = B^2/(2\mu_0)$). One min averages of the plasma and magnetic field data are used. We use $V_x > -100$ km/s near typical magnetopause locations to exclude magnetosheath crossings.

[8] We use the solar wind and IMF data mainly from Wind. The arrival time of the IMF at the subsolar bow shock at ($X = 17$, $Y = 0$, $Z = 0\ R_E$) is determined by calculating the minimum variance direction using the minimum variance analysis technique [*Weimer et al.*, 2003; *Weimer*, 2004]. During times when the Wind data is not available or the propagated Wind data is not reliable owing to the Wind's position (when Wind is more than ~50 R_E off the Sun-Earth line), we used the solar wind and IMF data from ACE, which is available after February 1998.

[9] To obtain plasma sheet particle content requires flux tube volume per unit magnetic flux, V. We estimate V using a formula based on a simple two-dimensional analytic model of plasma in force equilibrium [*Wolf et al.*, 2006]. The flux tube volume formula performs very well in tests involving force equilibrium magnetic field configurations with a RMS error ~0.16. The estimated V is used only when the perpendicular flow is slow ($V_\perp < 150$ km/s) and $\sqrt{(B_x^2 + B_y^2)}/B_z \leq 3$, a condition under which *Wolf et al.* found that their formula provides good estimates. Therefore, the estimated V will be more accurate than those obtained from empirical magnetic field models that do not take into account force balance.

[10] The objective of our study is to determine how particle content evolves after the IMF turns northward (southward) and stays northward (southward) afterward. For each plasma sheet data point measured at $t = t_0$, we examine the corresponding history of the past 13 h of the IMF angle θ between IMF B_y and B_z ($\theta \equiv sin^{-1}(B_z/B_{yz})$, where $B_{yz} = \sqrt{(B_y^2+B_z^2)}$). For each time history, we compute time averages of θ within two time periods: (1) θ_1 is the average over the time interval Δt before the measurement time (i.e., between $t = t_0$ and $t_0 - \Delta t$), where $\Delta t = 0, 1, 2, 3, 4, 5, 6, 7, 8$ h. (2) θ_2 is the average over the time interval Δt_2 before $t = t_0 - \Delta t$ (i.e., between $t = t_0 - \Delta t$ h and $t = t_0 - \Delta t - \Delta t_2$), where $\Delta t_2 = 1, 2, 3, 4, 5$ h. Evaluation of θ_2 allows to ensure that the plasma sheet has been mainly under northward (southward) IMF for a

Table 1. Ranges of θ_1 and θ_2 for Defining the Six Different IMF Conditions

	S IMF	N IMF	Weakly S IMF	Weakly N IMF	Strongly S IMF	Strongly N IMF
θ_1 (deg)	[−90, 0]	[0, 90]	[−15, 0]	[0, 15]	[−90, −15]	[15, 90]
θ_2 (deg)	[0, 90]	[−90, 0]	[0, 90]	[−90, 0]	[0, 90]	[−90, 0]

certain amount of time before IMF becomes southward (northward). In this paper, we show results mostly with Δt_2 = 4 h. The differences between the results with different Δt_2 and the reason to show those with Δt_2 = 4 h are discussed in 3.1. Table 1 lists the criteria for θ_1 and θ_2 for the six different IMF conditions we use to present our results. Note that since θ_1 and θ_2 are averages, the IMF direction may not actually remain in the same θ range continuously within the periods that θ_1 and θ_2 are obtained, so that each of the six IMF conditions should be considered as the IMF being predominantly directed in that particular direction range within the time intervals Δt and Δt_2.

3. Observational Results and Analysis

3.1. Evolution and Y Profiles of Particle Content Under S and N IMF

[11] Figure 1 shows how the plasma sheet properties at different Y locations between X = −20 and −30 R_E change with increasing Δt under the N and S IMF conditions (with Δt_2 = 4 h), and the number of 1 min measurements used in obtaining the statistical results. Note that because of our criteria for θ_2, the results at Δt = 0 for N IMF (S IMF) actually show a plasma sheet state that has been under S IMF (N IMF) for at least 4 h. At Δt = 0, plasma number density (n) is lower and temperature (T) is higher for the N than S IMF conditions because of the proceeding 4 h of the IMF being directed in the opposite direction. As Δt increases, n is seen to increase (decrease) and T to decrease (increases) for the N (S) IMF condition. After ~2 to 4 h following the IMF direction switch, n becomes higher and T lower for the N IMF than the S IMF condition. The above changes occur more quickly at smaller $|Y|$ (~2 h) than at larger $|Y|$ (~4 h). This indicates that the processes responsible for the above temporal changes are slow (of order of a few hours). The differences in n and T between the N and S IMF conditions are also larger at larger $|Y|$ (up to a factor > ~2.5 as seen at Y = −17.5 R_E) than at smaller $|Y|$ (up to a factor < ~1.5 as seen at Y = 2.5 R_E). For all the IMF conditions and for all Δt, n is always higher and T lower near the flanks than near midnight. In contrast to the significant changes of n and T in response to the IMF conditions, plasma pressure (p), for most Δt, is slightly higher during the S than N IMF conditions, and does not change substantially with increasing Δt for both the IMF conditions. There is also no strong Y dependence of p, unlike what are seen in n and T. That the changes of n only strongly affect T but not p indicates that particles associated with the changes seen in n, T, and p are mainly the colder plasma sheet particles that are below the plasma sheet thermal energy.

[12] The temporal and spatial variations of n can result from changes in flux tube particle content per unit magnetic flux (N) or/and in flux tube volume per unit magnetic flux (V) since $n = N/V$. As shown in Figure 1d, V in this X range is well correlated with p, with V being smaller when p is higher, but no good correlation is found between n and V. The variation of V with the IMF conditions is often not large compared to those of n and T (the largest change is less than 20%), and it has no strong dependence on Δt or the IMF direction. Thus the change of V is not sufficient to account for the density changes, so that the changes must be mainly due to the changes in N, as can be seen from Figures 1a and 1e the Y profiles, IMF dependences, and evolutions of N being very similar to those of n. Considering that the solar wind is the major particle source for the plasma sheet as indicated by the observed high correlations between the solar wind density and plasma sheet density [e.g., *Borovsky et al.*, 1997], the variations of N shown in Figure 1e could be simply a result of changes in the solar wind density. To correct for the effect of solar wind density, we normalize N to correspond to 5 cm^{-3} solar wind density ($N_{\rm norm} = 5 \cdot (n/n_{\rm sw})V$, where $n_{\rm sw}$ is the average of the solar wind density over Δt and 5 cm^{-3} is the typical solar wind density) as shown in Figure 1e. The close similarities between the N and $N_{\rm norm}$ profiles clearly indicate that change in the solar wind particle source is not the cause of the observed temporal and Y variations of plasma sheet particle content, and thus other processes are required to explain the changes of particle content.

[13] Figure 2a shows the Y profiles of $N_{\rm norm}$ at different Δt for the six IMF conditions listed in Table 1. It can be clearly seen that at any given time particle content is always smallest around midnight and becomes larger toward the flanks under all the IMF conditions, the profile resembling a "V" shape. Therefore, a spatial gradient of N pointed from midnight toward the flanks in the Y direction is always present in the plasma sheet. This gradient, as is discussed later, plays an important role in diffusing particles from the flanks toward midnight. Figure 2b shows the average rates of change of $N_{\rm norm}$ for Δt = 0 to 4 h and for Δt = 4 to 8 h. The changes for both N and S IMF are mostly quicker during the first few hours than during the later hours, and changes in the region of smaller $|Y|$ become very small during the later hours. When the IMF is more strongly northward or southward, the rate of change in the first 4 h is larger than for weakly northward or southward IMF. For the later hours, there is still substantial change near the flanks but essentially no change at smaller $|Y|$ for both strongly northward or southward IMF. The average increase rate in terms of density (assuming V to be a constant 2.5 R_E/nT) in the first 4 h of the N IMF condition is $dn/dt/n$~ 0.1 h^{-1}. This is similar to the increase rates observed by the low-latitude DMSP spacecraft [*Wing et al.*, 2005]. Note that dn/dt is larger in the work of *Wing et al.* [2005] because their densities are larger than the results shown in Figure 1a, which is likely due to the larger solar wind density (~10 cm^{-3}) during the period of their DMSP data.

[14] Figure 3 shows the temporal profiles of $N_{\rm norm}$ at different Y locations for θ_2 = 1 and 4 h. The particle content at Δt = 0 for the S IMF (N IMF) condition is lower (larger) for θ_2 = 1 h than for θ_2 = 4 h. However, regardless of the choice of θ_2, N increases or decreases quickly in the first ~4 h, and then the changes greatly slow down. Therefore, it takes ~4 h for the

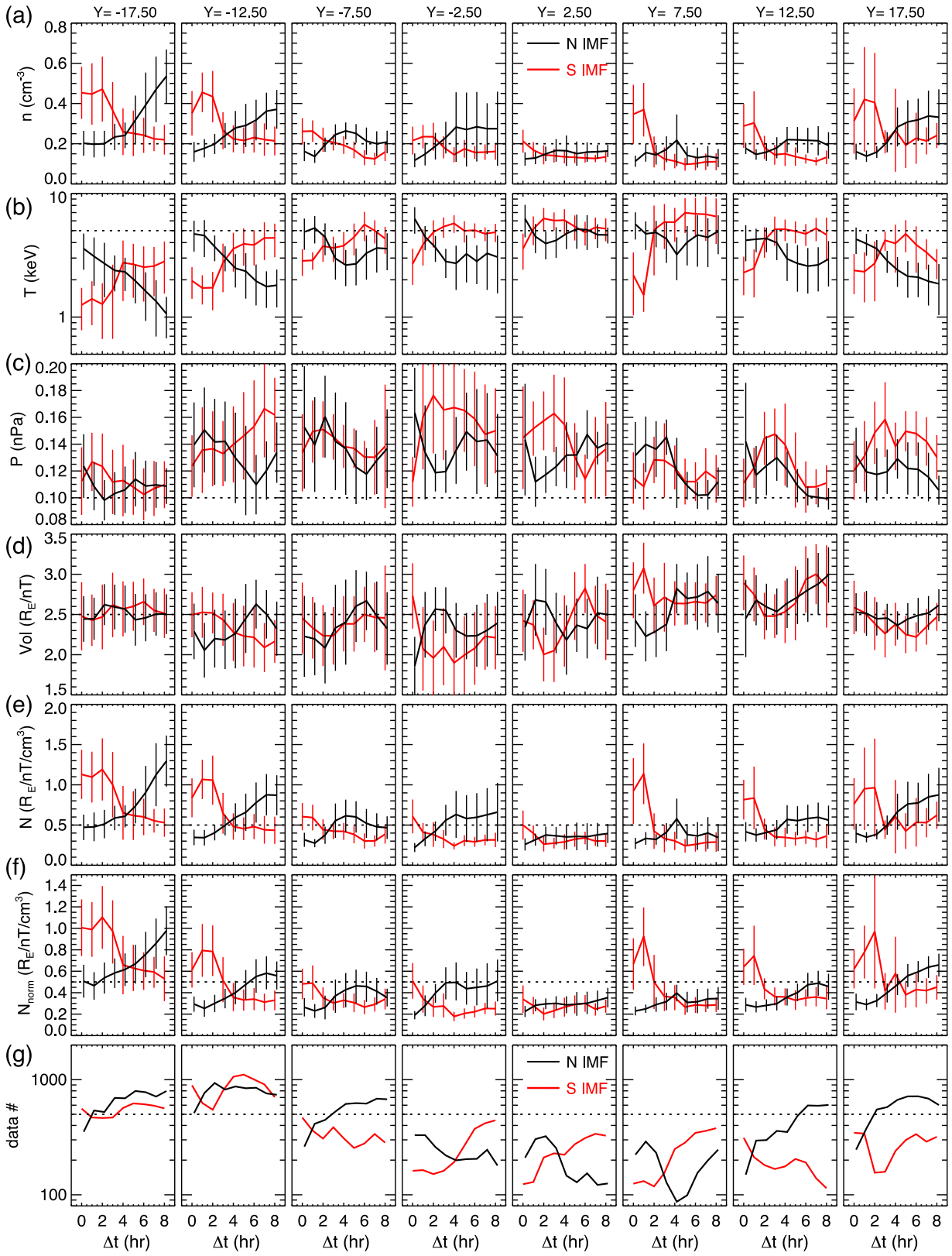

Figure 1. The temporal changes of the averages of (a) plasma sheet density, (b) plasma sheet temperature, (c) plasma sheet plasma pressure, (d) flux tube volume per unit magnetic flux, (e) plasma sheet particle content, (f) plasma sheet particle content normalized to corresponding to 5 cm^{-3} solar wind density, and (g) number of 1 min measurements for the northward (black curves) and southward (red curves) IMF with standard deviations (vertical lines) at different Y locations between $X = -20$ to -30 R_E.

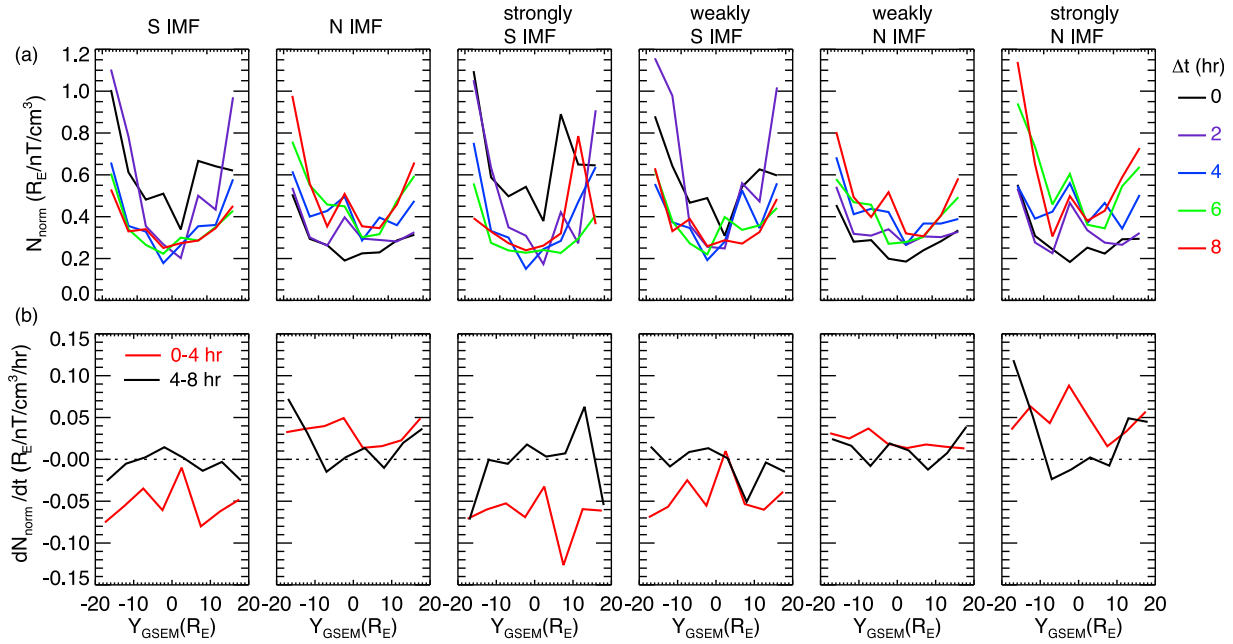

Figure 2. (a) Y profiles of the normalized plasma sheet content at different Δt and (b) rates of change of the normalized plasma sheet content averaged over $\Delta t = 0$ to 4 h (red curves) and 4 to 8 h (black curves) for the six different IMF conditions listed in Table 1.

plasma sheet to become substantially dense (tenuous) following the IMF becoming northward (southward). Thus we present results with $\theta_2 = 4$ h to better show the differences of N between the N and S IMF conditions.

[15] Considering a flux tube at a fixed location, an increase (decrease) of N indicates that there are more (less) particles entering this flux tube than those leaving. Particles can enter parallel from the ionosphere sources or leave parallel by precipitating into the ionosphere. However, ion precipitation losses in the plasma sheet are negligible and ionosphere sources are not strong during N IMF. During S IMF, there can be substantial particle entry from the ionosphere sources, but the sources may be sporadic and localized [e.g., *Wing and Johnson*, 2009]. Thus the above observed temporal and spatial variations of particle content should be largely associated with the particles entering or leaving the flux tube through perpendicular transport, which depends on factors such as spatial gradients of perpendicular transport (convergence or divergence), directions of transport, and locations of particle sources. During N IMF, the flanks are likely the only source locations. During S IMF, particles can also come from the mantles, but the flanks may still be a more important source for cold particles than the mantles. Therefore, determining what perpendicular transport processes are involved is the key to understanding the observed changes of particle content.

3.2. Plasma Drift and Fluctuations

[16] For particles sources located at the flanks, there have to be perpendicular transport processes to deliver the source particles toward midnight along the Y direction. Figure 4 shows the time series of plasma perpendicular bulk velocities at three different Y locations during 2 h periods of southward and northward IMF. Note that at $X < -20$ R_E the turbulence spatial scale (~10,000 km) and time scale (~140 s) [*Borovsky et al.*, 1997] are sufficiently larger than the gyroradius (~700 km for a 5 keV proton and B = 10 nT) and gyroperiod (~6 s for B = 10 nT) for the majority of plasma sheet protons so that a particle's motion across magnetic fields can be approximated with drift motion of the particle's guiding center. Therefore, in the region $-20 \geq X \geq -30$ R_E, it is valid to consider the observed perpendicular bulk

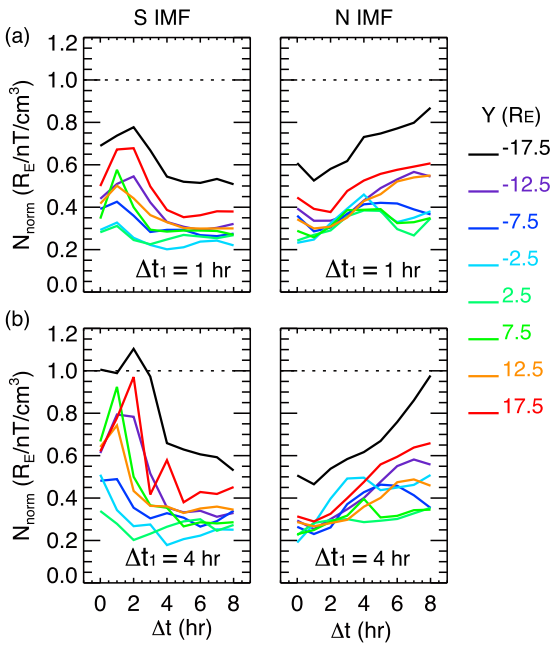

Figure 3. Temporal profiles of the normalized plasma sheet particle content at different Y locations for the northward and southward IMF conditions for two different criteria for Δt_1: (a) Δt_1 = 1 h and (b) Δt_1 = 4 h.

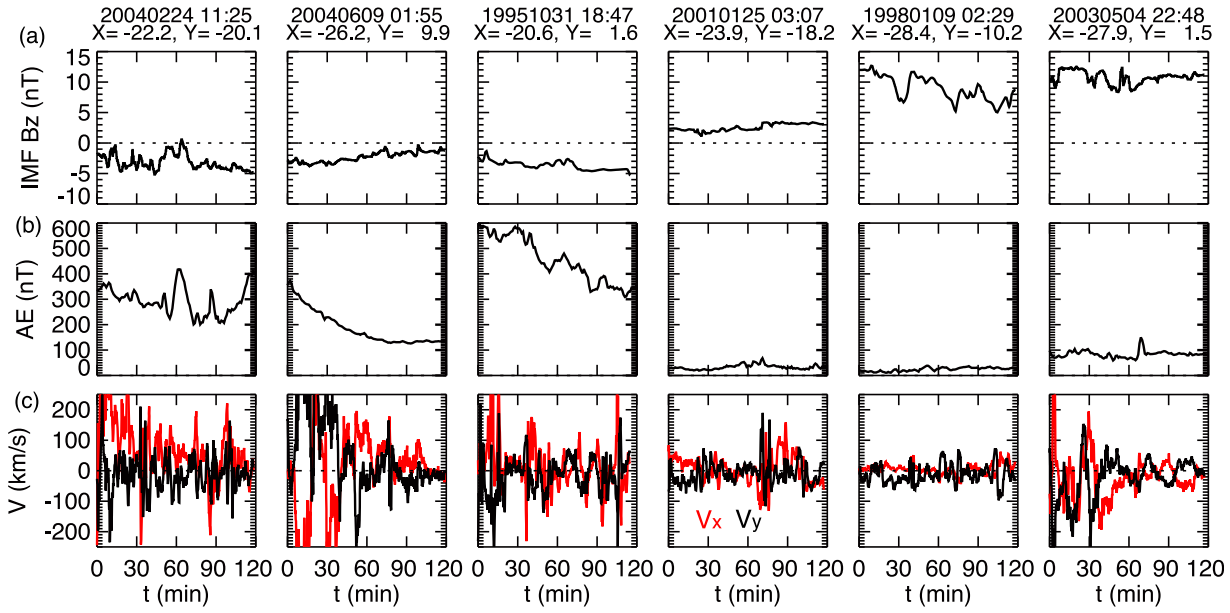

Figure 4. (a) IMF B_z, (b) AE, and (c) Geotail perpendicular velocities V_x and V_y for six different 2 h periods. The UT time at the start of each period ($t = 0$) and the Geotail positions at $t = 60$ min are indicated at the top of each plot.

velocity as drift velocity despite the plasma sheet being turbulent.

[17] It can be seen in Figure 4 that drift is not steady even during strongly N IMF with very low geomagnetic activity. Drift constantly changes both its magnitudes and directions in time scales up to about a few minutes, and the fluctuations are seen throughout the plasma sheet at all $|Y|$ locations. Despite drift being constantly fluctuating, Figure 5 shows that time average of drift has net earthward and flankward velocities. The average $|V_y|$ is as large as $|V_x|$, indicating that particles drift away from midnight as they drift earthward, which can result in loss of particles from the flux tubes near midnight. Because of this flankward component, the net drift without fluctuations cannot transport particles from the flank sources toward midnight to result in an increase of particle content at midnight, which suggests that other transport processes are involved.

[18] That drift constantly changes directions throughout the plasma sheet regardless of the IMF conditions and that sources at the flanks give a gradient of particle directed from midnight toward the flanks suggest that diffusive transport is a plausible candidate for moving particles across the tail toward midnight. Therefore, changes of particle content are likely a result of two transport processes: (1) particles leaving a flux tube owing to the net earthward and flankward drift, and (2) new particles from the flanks entering the flux tube owing to diffusive transport. The strength of diffusion depends on the magnitude of fluctuations, which is represented by a diffusion coefficient, as well as the magnitudes of spatial gradients. In order to evaluate how strong diffusive transport is relative to drift transport, we first estimate the diffusion coefficients associated with the observed fluctuating drift velocities.

3.3. Diffusion Coefficients

[19] *Borovsky et al.* [1997, 1998] estimated the diffusion coefficient D_{zz} associated with plasma sheet flows V_z to be 2.6×10^5 km^{2}s^{-1} using ISEE-2 data collected from 10 intervals during different geomagnetic activity levels. More recently, *Nagata et al.* [2008] computed the spatial distribution of D using Geotail data, but did not distinguish the flow direction and estimated D for the N IMF periods only. *Stepanova et al.* [2009] used Interball-Tail to obtain the spatial distribution of D_{yy} and D_{zz} for different substorm phases. The above results show that D is larger with increasing distance from the Earth, and is higher after a substorm onset than before the onset. In this study, we apply the methodology

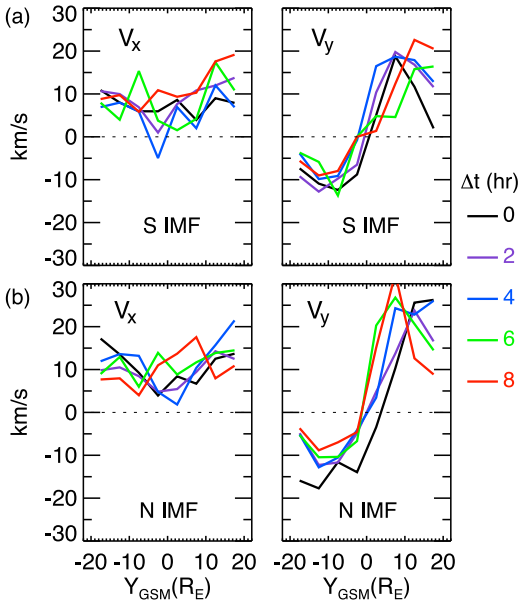

Figure 5. Y profiles of average perpendicular drift velocities V_x and V_y at different Δt for (a) the southward and (b) northward IMF conditions.

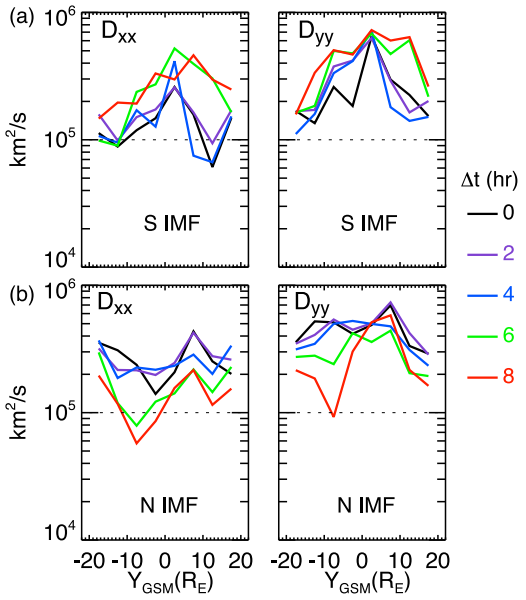

Figure 6. Y profiles of the diffusion coefficients D_{xx} and D_{yy} at different Δt for (a) the southward and (b) northward IMF conditions.

described in the work of *Borovsky et al.* [1997, 1998] to the Geotail data to compute the diffusion coefficients D_{xx} and D_{yy} associated with perpendicular drift $V_{\perp,x}$ and $V_{\perp,y}$, respectively, for the different IMF conditions.

[20] In the *Borovsky et al.* [1997] methodology, particle diffusion is assumed to be a Markov process (stochastic process), and the diffusion coefficient $D_{xx(yy)} = (V^2_{x(y),\mathrm{rms}} \cdot \tau_{x,\mathrm{auto}})/2$, where V_{rms} is the root mean square velocity and τ_{auto} is the autocorrelation time of V. τ_{auto} is a measure of the persistence of a fluctuating quantity and is computed from the autocorrelation function $\boldsymbol{A}$ ($\boldsymbol{A}(\tau) = (\int[V(t) - <V>][V(t+\tau) - <V>]dt)/(\int[V(t) - <V>][V(t) - <V>]dt)$). τ_{auto} in this study is defined as the value of the time shift where the $\boldsymbol{A}$ curve has fallen to the value of $1/e$, that is, $\boldsymbol{A}(\tau_{\mathrm{auto}}) = 1/e$. To compute τ_{auto} more accurately, we only select intervals during which Geotail is continuously within the central plasma sheet ($P_{\mathrm{ion}}/P_{\mathrm{mag}} \geq 2$) for 2 h to avoid the velocity changes owing to the satellite going in and out of the plasma sheet. Owing to this limitation, we only have enough data to obtain the dependence of τ_{auto} on the IMF direction but not Δt, so that we assume that τ_{auto} is independent of Δt. V_{rms} is computed from the probability distribution of drift velocities corresponding to the different IMF and Δt conditions.

[21] The Y profiles of $D_{xx(yy)}$ for the different IMF conditions and Δt are shown in Figure 6. $D_{xx(yy)}$ ranges from 10^5 to 10^6 km^2/s, consistent with the previous results [*Borovsky et al.*, 1998; *Nagata et al.*, 2008; *Stepanova et al.*, 2009]. D_{yy} is slightly larger than D_{xx} and both D_{yy} and D_{xx} decrease (increase) with increasing Δt for the N (S) IMF conditions. D_{xx} and D_{yy} is larger near midnight than near the flanks during S IMF, but have no clear Y dependences during N IMF.

4. Simulations of Drift and Diffusive Transport

[22] To evaluate the relative importance of drift and diffusive transport, we simulate the evolution of the spatial distribution of particle content owing to these two transport processes,

$$N(x,y,t) = N(x,y,t-\Delta t) + \Delta t \cdot \partial N(x,y,t-\Delta t)/\partial t, \quad (1)$$

where $\partial N/\partial t = -V_x \cdot \partial N/\partial x + \partial(D_{xx} \cdot \partial N/\partial x)/\partial x - V_y \cdot \partial N/\partial y + \partial(D_{yy} \cdot \partial N/\partial y)/\partial y$. The particle sources are assigned along the flanks and ionosphere losses and sources are not included.

4.1. Simulation Setups

[23] The simulation region is from $X = -20$ to -30 R_E and $Y = -20$ to 20 R_E, with grid spacing $\Delta X = \Delta Y = 0.1$ R_E. The dawn and dusk boundary conditions are specified along $Y = -20$ and 20 R_E, respectively, and the head and tail boundary conditions along $X = -20$ and -30 R_E, respectively. The flank boundary conditions are IMF- and time-dependent and are obtained from the Geotail observations shown in Figure 1f at $Y = -17.5$ (17.5) R_E for the dawn (dusk) flank. The flank boundary conditions represent the particle sources along the flanks. The Y profiles of V and D at different Δt for the different IMF conditions as shown in Figures 5 and 6 are used. The initial conditions represent a preexisting population and are the Y profiles for $\Delta t = 0$ shown in Figure 2a for the N and S IMF conditions. Since the initial and boundary conditions, and V and D are the averaged observations between $X = -20$ to -30 R_E, we assume that they are independent of X in the simulations.

[24] We use the tail boundary conditions to represent all the particles that first enter the plasma sheet from the flank sources located at $X < -30$ R_E and populate across the tail under the drift and diffusive transport in the Y direction, and then move earthward to $X = -30$ R_E. We also consider that the drift velocities and diffusion coefficients beyond $X = -30$ R_E can be different from those observed inside $X = -30$ R_E, so that these particles coming from the tail may experience changes in their transport as they enter the simulation region, which will thus alter their particle content distribution. We thus establish the time and Y-dependent tail boundary conditions by solving the equation (1) only in the Y direction, that is, $\partial N/\partial t = -C1 \cdot V_y \cdot \partial N/\partial y + \partial(C2 \cdot D_{yy} \cdot \partial N/\partial y)/\partial y$, where $C1$ and $C2$ are constants and are added to allow adjustment of the drift speed and the diffusion coefficients. The time-dependent V_y, D_{yy}, and the boundary conditions at $Y = \pm 20$ R_E used in establishing the tail boundary conditions are the same as those used inside the simulation region. Therefore, the tail boundary conditions established are strongly affected by the changes in the flank conditions. When $C1 \neq 1$ or $C2 \neq 1$, the distribution of N associated with the particles from the tail boundary is expected to change because of the changes of drift from $C1 \cdot V_y$ to V_y, and of diffusion coefficient from $C2 \cdot D_{yy}$ to D_{yy}. For example, if $C1 < 1$ and $C2 = 1$, the particles from the tail boundary, as they enter the model region, will be affected by flankward drift stronger than that beyond $X = -30$ R_E, and will thus be pushed further away from midnight as they move from $X = -30$ to -20 R_E. Since there are almost no Geotail observations beyond $X = -30$ R_E available for obtaining realistic V and D, we have run simulations with different $C1$ and $C2$ to investigate how they can affect the simulation results. As discussed in 4.2, the values of $C1$ and $C2$ that give the best agreement with observations are as

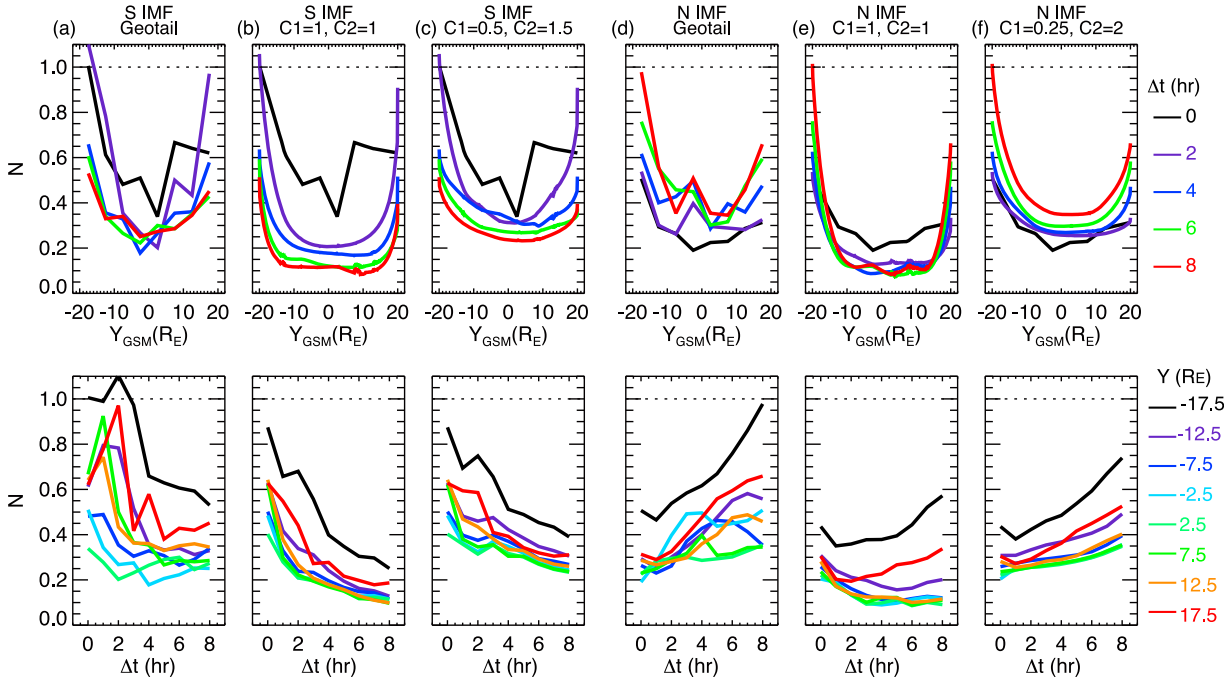

Figure 7. Comparisons between the Geotail observations and the simulation results with different tail boundary conditions for the (a–c) southward and (d–f) northward IMF conditions. The Y profiles of particle content at different Δt (top panels) and the temporal profiles at different Y locations (bottom panels) are shown.

expected from the changes of V_y and D_{yy} with increasing X that have been previously observed inside $X = -30\ R_E$ [*Wang et al.*, 2009; *Stepanova et al.*, 2009].

[25] Compared with the tail boundary conditions, the head boundary condition along $X = -20\ R_E$ is not as important to the simulation results since drift is earthward. We assume that the head boundary conditions are time-dependent but are constant in Y with values of the smallest N_{norm} at each Δt as shown in Figure 1f. (We have also run simulations with Y-dependent head boundary conditions and found that the results are similar to those with no Y dependence.) We have run the simulation for both the S and N IMF conditions for 8 simulation hours with a fixed time step of 400 s.

[26] In the simulations, we use the operator splitting method with the fifth-order Runge-Kutta method for computing the drift transport and the Crank-Nicolson method for the diffusive transport. We use the alternating-direction implicit method when using the Crank-Nicolson method to solve the 2-D diffusion, which is second-order accurate in space and time, and unconditionally stable. As discussed in Appendix A, we tested our numerical schemes in a convection-diffusion problem with known analytical solutions and the RMS error is ~5%. Therefore, our schemes are able to largely suppress errors owing to numerical diffusion.

4.2. Simulation Results and Discussions

[27] The simulation results averaged over $X = -21$ to $-29\ R_E$ with different tail boundary conditions are shown in Figure 7. For the S IMF simulations, despite the diffusion coefficients becomes slightly larger with increasing Δt, diffusive transport becomes weaker with increasing Δt mainly because of the significant decrease of the flank sources. The weakening diffusive transport thus brings fewer new particles into the plasma sheet. At the same time, the preexisting particles built up during the proceeding N IMF period drift away from midnight. As a result, N decreases quickly in the first 2 to 4 h but the decrease slows down afterward. The slowing down is due to the changes in the Y profile, as it evolves from a "V" shape toward a more "U" shape. Compared with a "V" profile, a "U" profile has a stronger Y gradient, thus a larger diffusive transport, at larger $|Y|$ locations. Therefore, the evolution toward a "U" shape makes the difference between the drift and diffusive transport become smaller, thus slowing down the change of N. For the results with $C1 = C2 = 1$, the decrease of N outside $|Y| = 10\ R_E$ is too large compared with the Geotail observations. The results with $C1 = 0.5$ and $C2 = 1.5$, which assumes $|V_y|$ is weaker and diffusion is stronger in the more distant tail, agree much better with the observations both in their spatial and temporal profiles. Despite not considering particles coming from the ionosphere or the mantles in the simulations, the above agreements suggest that the flank is still a major source for the plasma sheet particle content during S IMF compared with the ionosphere and mantles.

[28] For the N IMF simulations with $C1 = C2 = 1$, N increases with increasing Δt only in the region outside $|Y| \sim 10\ R_E$. The increase is mainly due to more new particles coming from the flanks because of strengthening diffusive transport resulting from the increasing flank sources with Δt. However, the number of new particles brought inside $|Y| \sim$

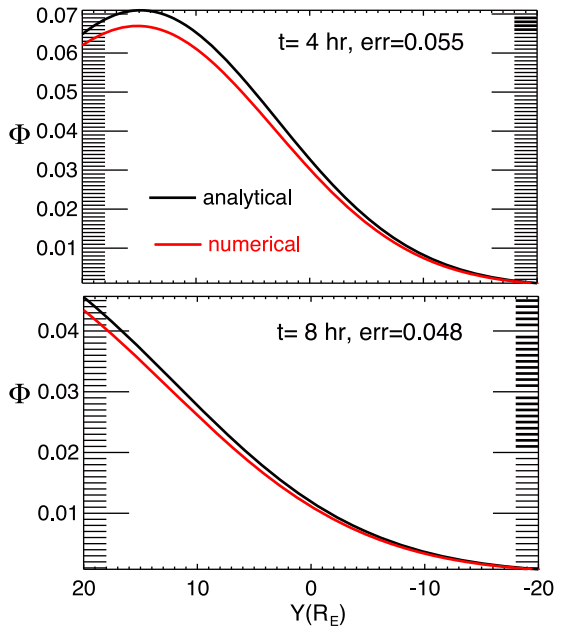

Figure 8. Comparisons between the analytic solutions (black curves) and the numerical solutions (red curves) at (top) $t = 4$ and (bottom) $t = 8$ h.

10 R_E by the increasing diffusion is still less than the number of particles drifting away from midnight. But when considering D to be stronger and Vy to be weaker in the region tailward of $X = -30$ R_E, as shown by the results with $C1 = 0.25$ and $C2 = 2$, there is substantial particle increase inside $|Y| = 10$ R_E, and the temporal evolution and the Y profile of N agree much better with the observations. Since $|V_y|$ is stronger inside than outside $|Y| \sim 10$ R_E, the rate of increase of N is smaller at smaller $|Y|$, which is also consistent with the observations.

[29] Among the simulation results that we have tried with different $C1$ and $C2$ values, those shown in Figures 7c and 7f have the best agreement with the observations in both temporal and Y profiles. Despite there being no observations available to verify if these $C1$ and $C2$ values are realistic, previous observations inside $X = -30$ R_E show that D_{yy} increases [*Stepanova et al.*, 2009] while $|V_y|$ decreases [*Wang et al.*, 2009] with increasing X with D_{yy} ($|V_y|$) at $X = -25$ R_E being a factor of ~2 higher (lower) than that at $X = -15$ R_E. Our best $C1$ and $C2$ values are consistent with the expectation inferred from the X variations of $|V_y|$ and D_{yy}.

[30] The simulations indicate that the observed temporal and Y variations of plasma sheet particle content can be accounted for by the competition between the particle increase owing to diffusive transport of particles from the flank sources and the particle decrease owing to flankward drift transport. As the IMF B_z switches directions, the flank sources change very significantly while the drift velocities and diffusion coefficients do not change as much. Therefore, it is mainly the increase (decrease) of the flank sources during N (S) IMF that makes the particle increase by diffusive transport become larger (smaller) than the particle decrease owing to drift, thus resulting in a net increase (decrease) of plasma sheet particle content.

[31] Our results, however, do not rule out other possible transport processes. For example, MHD simulations show that the particles that enter to the plasma sheet from the magnetosheath can have relatively lower entropy than the surrounding plasma sheet plasma, which can move further toward midnight and earthward owing to interchange instability (J. Lyon, personal communication, 2009). Some event studies using Geotail show that the cold population can suddenly disappear when there is a substorm, which may be involved with reconnection in the tail. These other processes may be associated with more transient or smaller-scale transport, while the drift and diffusive transports appear to be responsible for the changes on larger temporal and spatial scales.

5. Summary

[32] We have statistically analyzed 11 years of Geotail data to investigate the underlying processes that result in colder and denser plasma sheet during N IMF than during S IMF. There are significant differences in the plasma sheet number density and temperature between the N and S IMF conditions, but not in the plasma sheet pressure and flux tube volume per unit flux, indicating that the change of plasma sheet state with the IMF B_z direction is mainly due to change of plasma sheet content per unit magnetic flux (N) and that N is contributed mostly by cold plasma sheet particles. N decreases (increases) as the S IMF (N IMF) period becomes longer. The change is quicker in the first 2–4 h but slows down substantially afterward. N varies significantly across the tail under all the IMF conditions with higher values near the flanks than near midnight. These temporal and spatial variations of N are not due to changes of the solar wind density.

[33] Drift velocities are observed to be constantly fluctuating in magnitude and direction throughout the plasma sheet for all IMF conditions. Analysis of the observations suggests that plasma sheet particles can undergo two transport processes: a net earthward and flankward drift, and diffusive transport resulting from the fluctuations. Drift speeds are < ~20 km/s and the diffusion coefficients are estimated to be ~10^5 to 10^6 km^2/s. Considering the flanks being the major source location for cold particles, diffusive transport can bring the source particles across the tail and deep into midnight plasma sheet. Drift transport, on the other hand, pushes particles across the tail away from midnight. The change of particle content, therefore, is likely a result of the competition between the decrease owing to drift and the increase owing to diffusive transport.

[34] Simulations are conducted to evaluate the change of N owing to diffusive and drift transport, with IMF and time-dependent flank particle sources, drift velocities, and diffusion coefficients based on the Geotail observations. The good agreements between the observations and simulation results indicate that the observed temporal and Y variations of N can be account for by the drift and diffusive transport of particles from the flank sources. As the IMF B_z switches direction, it is mainly the increase (decrease) of the flank sources during N (S) IMF that makes the particle increase by diffusive transport become larger (smaller) than the particle decrease owing to

drift, thus resulting in a net increase (decrease) of plasma sheet particle content.

Appendix A

[35] Considering the evolution of a Gaussian pulse Φ owing to convection and diffusion

$$\partial\Phi/\partial t = -V_x \cdot \partial\Phi/\partial x - V_y \cdot \partial\Phi/\partial y + D_{xx} \cdot \partial^2\Phi/\partial x^2 + D_{yy} \cdot \partial^2\Phi/\partial^2,$$

with an initial condition,

$$\Phi(0,x,y) = \exp\left(-\frac{(x-0.5)^2}{D_{xx}} - \frac{(y-0.5)^2}{D_{yy}}\right).$$

Φ has an analytic solution [e.g., *Karaa and Zhang*, 2004],

$$\Phi(t,x,y) = \frac{1}{4t+1}\exp\left(-\frac{(x-V_x t-0.5)^2}{D_{xx}(4t+1)} - \frac{(y-V_y t-0.5)^2}{D_{yy}(4t+1)}\right).$$

Using the numerical schemes described in 4.1, we solved the evolution of $\Phi(t, x, y)$ numerically for 8 simulation hours within $X = [-20, -30]\ R_E$ and $Y = [-20, 20]\ R_E$, with $\Delta X = \Delta Y = 0.1\ R_E$, $\Delta t = 400$ s. We used $V_x = V_y = 0.001\ R_E$/s (~7 km/s) and $D_{xx} = D_{yy} = 0.005\ R_E^2$/s (~$5 \cdot 10^5$ km^2/s), which are the typical values in the plasma sheet. The time-dependent boundary conditions are given by the analytic solution. Figure 8 shows the comparisons between the results from the analytic solution and from our simulations at $t = 4$ and 8 h. The RMT error is 5.5 and 4.8%.

[36] **Acknowledgments.** The work by C.-P. Wang and L. R. Lyons has been supported by NASA grant NNX07AF66G, NNX07AG42G, and NNX08A135G, and NSF grant ATM-0819864. The work by J. M. Weygand has been supported by a Space Weather grant ATM 02-08501, by NASA Research at 1 AU grant NG-04GA93G, and NASA grant NNX07AC93G. The work by A. T. Lui has been supported by NSF grant ATM-0630912. We thank T. Mukai at ISAS and CDAWeb for the use of the Geotail LEP data. The Geotail magnetic field data are provided through the DARTS system by ISAS. We thank Jon Vandegriff of the Applied Physics Laboratory for providing the Geotail EPIC data. We also thank Dan Weimer for providing the Weimer variance analysis routine.

[37] Masaki Fujimoto thanks Elizaveta Antonova for her assistance in evaluating this paper.

References

Angelopoulos, V., et al. (1993), Characteristics of ion flow in the quiet state of the inner plasma sheet, *Geophys. Res. Lett.*, *20*, 1711–1714, doi:10.1029/93GL00847.

Antonova, E. E. (2006), Quasiturbulent transport and LLBL properties, *Adv. Space Res.*, *37*, 532–536, doi:10.1016/j.asr.2006.01.019.

Borovsky, J., R. C. Elphic, H. O. Funsten, and M. F. Thomsen (1997), The Earth's plasma sheet as a laboratory for flow turbulence in high-[beta] MHD, *J. Plasma Phys.*, *57*, 1–34, doi:10.1017/S0022377896005259.

Borovsky, J. E., M. F. Thomsen, and R. C. Elphic (1998), The driving of the plasma sheet by the solar wind, *J. Geophys. Res.*, *103*, 17,617–17,639, doi:10.1029/97JA02986.

Chen, M. W., C.-P. Wang, M. Schulz, and L. R. Lyons (2007), Solar-wind influence on MLT dependence of plasma sheet conditions and their effects on storm time ring current formation, *Geophys. Res. Lett.*, *34*, L14112, doi:10.1029/2007GL030189.

Fujimoto, M., and T. Terasawa (1994), Anomalous ion mixing within an MHD-scale Kelvin-Helmholtz vortex, *J. Geophys. Res.*, *99*, 8601–8613, doi:10.1029/93JA02722.

Gkioulidou, M., C.-P. Wang, L. R. Lyons, and R. A. Wolf (2009), Formation of the Harang reversal and its dependence on plasma sheet conditions: Rice convection model simulations, *J. Geophys. Res.*, *114*, A07204, doi:10.1029/2008JA013955.

Johnson, J. R., and C. Z. Cheng (1997), Kinetic Alfvén waves and plasma transport at the magnetopause, *Geophys. Res. Lett.*, *24*, 1423–1426, doi:10.1029/97GL01333.

Karaa, S., and J. Zhang (2004), High order ADI method for solving unsteady convection-diffusion problems, *J. Comput. Phys.*, *198*, 1–9, doi:10.1016/j.jcp.2004.01.002.

Kokubun, S., T. Yamamoto, M. H. Acuna, K. Hayashi, K. Shiokawa, and H. Kawano (1994), The Geotail magnetic field experiment, *J. Geomagn. Geoelectr.*, *46*, 7–21.

Lavraud, B., M. F. Thomsen, J. E. Borovsky, M. H. Denten, and T. I. Pulkkinen (2006), Magnetosphere preconditioning under northward IMF: Evidence from the study of coronal mass ejection and corotating interaction region geoeffectiveness, *J. Geophys. Res.*, *111*, A09208, doi:10.1029/2005JA011566.

Lavraud, B., and V. K. Jordanova (2007), Modeling the effects of cold-dense and hot-tenuous plasma sheet on proton ring current energy and peak location, *Geophys. Res. Lett.*, *34*, L02102, doi:10.1029/2006GL027566.

Li, W., J. Raeder, M. F. Thomsen, and B. Lavraud (2008), Solar wind plasma entry into the magnetosphere under northward IMF conditions, *J. Geophys. Res.*, *113*, A04204, doi:10.1029/2007JA012604.

Mukai, T., S. Machida, Y. Saito, M. Hirahara, T. Terasawa, N. Kaya, T. Obara, M. Ejiri, and A. Nishida (1994), The low-energy particle (LEP) experiment onboard the Geotail satellite, *J. Geomagn. Geoelectr.*, *46*, 669–692.

Nagata, D., S. Machida, S. Ohtani, Y. Saito, and T. Mukai (2008), Solar wind control of plasma number density in the near-Earth plasma sheet: Three-dimensional structure, *Ann. Geophys.*, *26*, 4031–4049.

Øieroset, M., T. D. Phan, M. Fujimoto, L. Chan, R. P. Lin, and R. Skoug (2003), Spatial and temporal variations of the cold dense plasma sheet: Evidence for a low-latitude boundary layer source?, in *Earth's Low-Latitude Boundary Layer*, *Geophys. Monogr. Ser.*, vol. 133, edited by P. T. Newell and T. Onsager, pp. 53–62, AGU, Washington, D. C.

Otto, A., and K. Nykyri (2003), Kelvin-Helmholtz instability and magnetic reconnection: Mass transport at the LLBL, in *Earth's Low-Latitude Boundary Layer*, *Geophys. Monogr. Ser.*, vol. 133, edited by P. T. Newell and T. Onsager, pp. 53–62, AGU, Washington, D. C.

Ovchinnikov, I. L., E. E. Antonova, and Y. I. Yermolaev (2000), Determination of the turbulent diffusion coefficient in the plasma sheet using the project INTERBALL data, *Cosmic Res., Engl. Transl.*, *38*, 557–561, doi:10.1023/A:1026686600686.

Song, P., and C. T. Russell (1992), Model of the formation of the low-latitude boundary layer for strongly northward interplanetary magnetic field, *J. Geophys. Res.*, *97*, 1411–1420, doi:10.1029/91JA02377.

Spence, H. E., and M. G. Kivelson (1993), Contributions of the low-latitude boundary layer to the finite width magnetotail convection model, *J. Geophys. Res.*, *98*, 15,487−15,496, doi:10.1029/93JA01531.

Stepanova, M., E. E. Antonova, D. Paredes-Davis, I. L. Ovchinnikov, and Y. I. Yermolaev (2009), Spatial variation of eddy-diffusion coefficients in the turbulent plasma sheet during substorms, *Ann. Geophys.*, *27*, 1407–1411.

Terasawa, T., et al. (1997), Solar wind control of density and temperature in the near-Earth plasma sheet: WIND/GEOTAIL collaboration, *Geophys. Res. Lett.*, *24*, 935–938, doi:10.1029/96GL04018.

Wang, C.-P., L. R. Lyons, M. W. Chen, and F. R. Toffoletto (2004), Modeling the transition of the inner plasma sheet from weak to enhanced convection, *J. Geophys. Res.*, *109*, A12202, doi:10.1029/2004JA010591.

Wang, C.-P., L. R. Lyons, J. M. Weygand, T. Nagai, and R. W. McEntire (2006), Equatorial distributions of the plasma sheet ions, their electric and magnetic drifts, and magnetic fields under different interplanetary magnetic field Bz conditions, *J. Geophys. Res.*, *111*, A04215, doi:10.1029/2005JA011545.

Wang, C.-P., L. R. Lyons, T. Nagai, J. M. Weygand, and R. W. McEntire (2007), Sources, transport, and distributions of plasma sheet ions and electrons and dependences on interplanetary parameters under northward interplanetary magnetic field, *J. Geophys. Res.*, *112*, A10224, doi:10.1029/2007JA012522.

Wang, C.-P., L. R. Lyons, R. A. Wolf, T. Nagai, J. M. Weygand, and A. T. Y. Lui (2009), The plasma sheet PV5/3 and nV and associated plasma and energy transport for different convection strengths and AE levels, *J. Geophys. Res.*, *114*, A00D02, doi:10.1029/2008JA013849.

Weimer, D. R. (2004), Correction to "Predicting interplanetary magnetic field (IMF) propagation delay times using the minimum variance technique", *J. Geophys. Res.*, *109*, A12104, doi:10.1029/2004JA010691.

Weimer, D. R., D. M. Ober, N. C. Maynard, M. R. Collier, D. J. McComas, N. F. Ness, C. W. Smith, and J. Watermann (2003), Predicting interplanetary magnetic field (IMF) propagation delay times using the minimum variance technique, *J. Geophys. Res.*, *108*(A1), 1026, doi:10.1029/2002JA009405.

Williams, D. J., R. W. McEntire, C. Schlemm II, A. T. T. Lui, G. Gloeckler, S. P. Christon, and F. Gliem (1994), GEOTAIL energetic particles and ion composition instrument, *J. Geomagn. Geoelectr.*, *46*, 39–57.

Wing, S., and J. R. Johnson (2009), Substorm entropies, *J. Geophys. Res.*, *114*, A00D07, doi:10.1029/2008JA013989.

Wing, S., and P. T. Newell (2002), 2D plasma sheet ion density and temperature profiles for northward and southward IMF, *Geophys. Res. Lett.*, *29*(9), 1307, doi:10.1029/2001GL013950.

Wing, S., J. R. Johnson, P. T. Newell, and C.-I. Meng (2005), Dawn-dusk asymmetries, ion spectra, and sources in the northward interplanetary magnetic field plasma sheet, *J. Geophys. Res.*, *110*, A08205, doi:10.1029/2005JA011086.

Wolf, R. A., V. Kumar, F. R. Toffoletto, G. M. Erickson, A. M. Savoie, C. X. Chen, and C. L. Lemon (2006), Estimating local plasma sheet PV5/3 from single-spacecraft measurements, *J. Geophys. Res.*, *111*, A12218, doi:10.1029/2006JA012010.

A. T. Y. Lui, Applied Physics Laboratory, Johns Hopkins University, Space Department, 11100 Johns Hopkins Rd., Laurel, MD 20723, USA.

L. R. Lyons and C.-P. Wang, Department of Atmospheric and Oceanic Sciences, University of California, 405 Hilgard Ave., 7127 Math Sciences, Los Angeles, CA 90095, USA. (cat@atmos.ucla.edu)

T. Nagai, Department of Earth and Planetary Sciences, Tokyo Institute of Technology, Ookayama 2-12-1 Meguro, 12-5 Tokyo, 152-8551, Japan.

J. M. Weygand, Institute of Geophysics and Planetary Physics, University of California, 3845 Slichter Hall, 405 Charles E. Young Dr., PO Box 951567, Los Angeles, CA 90095, USA.